Regenerative Therapy 26 (2024) 999–1009

Contents lists available at ScienceDirect

Regenerative Therapy

journal homepage: http://www.elsevier.com/locate/reth

Original Article

Unveiling the superior function of RADA in bone regeneration compared to KSL as two critical cores within self-assembling peptide nanofibers: Insights from in vitro and in vivo studies

Bita Rasoulian [a, b], Zahra Sheikholislam [c], Mohammad Hassan Houshdar Tehrani [c], Solmaz Chegeni [a], Elham Hoveizi [d], Seyed Mahdi Rezayat [e, f], Shima Tavakol [a, g, *]

[a] Cellular and Molecular Research Center, Iran University of Medical Sciences, Tehran, Iran
[b] School of Biomedical Sciences, Vrije Universiteit Amsterdam, Amsterdam, the Netherlands
[c] Department of Medicinal Chemistry, School of Pharmacy, Shahid Beheshti University of Medical Sciences, Tehran, Iran
[d] Department of Biology, Faculty of Science, Shahid Chamran University of Ahvaz, Ahvaz, Iran
[e] Department of Medical Nanotechnology, Tehran University of Medical Sciences, Tehran, Iran
[f] Department of Pharmacology, School of Medicine, Tehran University of Medical Sciences, Tehran, Iran
[g] Department of Research and Development, Tavakol BioMimetic Technologies Company, Tehran, Iran

ARTICLE INFO

Article history:
Received 9 August 2024
Received in revised form
12 September 2024
Accepted 25 September 2024

Keywords:
Self-assembling peptide nanofiber
Cell signaling
Core of self-assembly
KSL
Osteogenesis
Bone mineral density

ABSTRACT

Introduction: Self-assembling peptide nanofibers have emerged as promising biomaterials in the realm of bone tissue engineering due to their biocompatibility, biodegradability, and ability to mimic the native extracellular matrix. This study delved into the comparative efficacy of two distinct self-assembling peptide nanofibers, RADA-BMHP1 and KSL-BMHP1, both incorporating the biological motif of BMHP1, but differing in their core peptide sequences.

Methods: Cell viability and osteogenic differentiation in rat mesenchymal stem cells (rMSCs), and bone regeneration in rat were compared.

Results: In vitro assays revealed that KSL-BMHP1 promoted enhanced cell viability, and nitric oxide production than RADA-BMHP1, an effect potentially attributable to its lower hydrophobicity and higher net charge at physiological pH. Conversely, RADA-BMHP1 induced superior osteogenic differentiation, evidenced by upregulation of key osteogenic genes, increased alkaline phosphatase activity (ALP), and enhanced matrix mineralization which may be attributed to its higher protein-binding potential and grand hydropathy, facilitating interactions between the peptide nanofibers and proteins involved in osteogenesis. In vivo experiments utilizing a rat bone defect model demonstrated that both peptide nanofibers improved bone regeneration at the genes level and ALP activity, with RADA-BMHP1 exhibiting a more pronounced increase in bone formation compared to KSL-BMHP1. Histological evaluation using H&E, Masson's trichrome and Wright-Giemsa staining confirmed the biocompatibility of both nanofibers.

Conclusion: These findings underscore the pivotal role of the core structure of self-assembling peptide nanofibers, beyond their biological motif, in the fate of tissue regeneration. Further research is warranted to optimize the physicochemical properties and functionalization of these nanofibers to enhance their efficacy in bone regeneration applications.

1. Introduction

Bone grafts are biomaterials used to replace or repair missing or damaged bone tissue. They can be categorized into four main types: autografts, allografts, xenografts, and synthetic grafts. Alloplastic bone grafts, also known as synthetic bone grafts or bone graft substitutes, designed to promote bone healing and regeneration.

* Corresponding author. Cellular and Molecular Research Center, Iran University of Medical Sciences, Tehran, 1449614535, Iran.
E-mail address: shima.tavakol@yahoo.com (S. Tavakol).

Peer review under responsibility of the Japanese Society for Regenerative Medicine.

https://doi.org/10.1016/j.reth.2024.09.010

They are used as an alternative to autografts, allografts, and xenografts in bone grafting procedures. The primary materials used in alloplastic grafts include hydroxyapatite, tricalcium phosphate, bioactive glass, and various types of polymers. Current knowledge highlights the advantages and disadvantages of each graft type. Autografts are considered the gold standard, offering the best osteoinductive, osteoconductive, and osteogenic properties. However, they are limited by donor site morbidity and insufficient supply. Allografts and xenografts can provide larger volumes of graft material, but they carry the risk of disease transmission and can elicit an immune. Alloplastic grafts offer several advantages, such as the elimination of donor site morbidity, unlimited availability, no risk of disease transmission, and reduced risk of immune rejection. However, they generally exhibit inferior biological properties compared to autografts, as they lack the inherent osteoinductive and osteogenic properties found in natural bone tissue. Notwithstanding, the incorporation of biological motifs into the structure of alloplastic polymers eliminates this obstacle [1].

Allografts made up a substantial part of the market due to their widespread use and acceptance in various orthopedic procedures. Alloplastic materials, on the other hand, were gaining popularity due to their potential to overcome some limitations of autografts, allografts, and xenografts, as well as advancements in material science and regenerative medicine. The global market share of bone substitutes in 2022 was $3.2 billion, which is expected to reach $ 6.3 billion by 2032 [2]. Among these, 44 % of the market is related to synthetic bone substitutes (alloplastic). This growth can be attributed to factors such as an aging population, increasing prevalence of orthopedic disorders, advances in bone graft technologies, and growing awareness about the benefits of synthetic and alloplastic bone graft materials. In Europe, according to a study, the market share of synthetic bone substitutes has grown by 134.4 %, which is higher than the growth rate of allografts. In fact, bone is the second most transplanted tissue after blood in the world.

According to the FDA database, 87 alloplastic bone graft products have been approved in the United States since 1996. According to the Drug and Medical Device Agency database, 10 alloplastic bone graft products have been approved in Japan since 2004. According to the Ministry of Health and Welfare database, 36 alloplastic bone graft products have been approved in Korea since 1980. Among the products produced in America, TRICOS products containing fibrin matrix, SynOss collagen synthetic material (SynOss Putty) and Mastergraft containing collagen, Easy-graft containing PLGA, Healos dental bone graft substitute containing bovine collagen, ReOss containing PLGA, NovaBone Dental Contains polyethylene glycol, PerioGlas contains gelatin, Osteocaf contains PLGA. The polymer component of these products is collagen, gelatin, polyethylene glycol and PLGA. In the production of alloplastic products, only one of these products with the ReFit Dental brand name uses natural polymers in addition to ceramics, and the rest of the compounds are ceramic. In Korean products, Ossbone Collagen, DualPor Collagen D-Injection, and Osteon II and III Collagen contain pig and cow collagen, which again have problems related to extraction from animal tissues, such as the extraction process, the possibility of disease transmission and infection.

Hydrogel-based scaffolds have potential as a substitute for solid calcium-phosphate materials such as hydroxyapatite and tricalcium phosphate, which lack the ability to encapsulate cells [3]. Hydrogel-based scaffolds can effectively fill cavities and defects, and integrate well across damaged areas. These scaffolds have a distinctive characteristic of mimicking the physiological environment by creating a 3D extracellular matrix with high pore interconnectivity and the ability to encapsulate cells [4].

Self-assembling peptide nanofibers, a type of hydrogel-based scaffold, have been developed for clinical use, such as PuraMatrix® BVF, which serves as a dental and sinus bone filler [5]. These peptide nanofiber scaffolds possess advantages in terms of both bioactive motifs and nanotopographical structures. Various studies have reported that nanotopography plays a crucial role in osteogenesis from adhesion to differentiation [6–8] For instance, Yang et al. demonstrated that nanotopography promotes colocalization of bone morphogenic protein receptor 1 A (BMPR1A) and integrins, which leads to the expression of RUNX2 gene and ultimately facilitates osteogenesis [6].

Self-assembling peptide nanofibers have gained significant attention as a promising biomaterial due to their potential applications in a range of clinical settings, including tissue engineering, drug delivery, and regenerative medicine, because of their unique properties, including biocompatibility, biodegradability, and the ability to self-assemble into three-dimensional structures. Self-assembling peptide nanofibers can mimic the natural extracellular matrix (ECM) of bone tissue, providing a suitable environment for cell adhesion, proliferation, and differentiation. This can lead to enhanced tissue regeneration and healing compared to traditional bone graft materials. They are highly versatile and can be engineered to exhibit specific properties, such as mechanical strength, degradation rate, and bioactivity. This allows for customization of the material to suit specific applications and clinical needs.

While much progress has been made in understanding the properties of peptide nanofibers and their potential applications, there is still much to learn about these materials and their clinical utility. One area of ongoing research is the development of new peptide sequences and methods for controlling the properties of peptide nanofibers. Researchers are exploring new ways to tune the chemical, and biological properties of peptide nanofibers to optimize their performance in specific applications. They have repetitive amino acid sequences as the core like RADA and KSL, which are in a sol state, but transform into hydrogel-based scaffolds with β-sheet structures and nanofiber topography when exposed to ionic media. These scaffolds also contain bioactive motifs, such as laminin's IKVAV [9,10], fibronectin's RGD, and bone marrow homing peptide 1 (BMHP1) with the sequence PFSSTKT [11], which facilitate cell-cell interactions crucial for osteogenesis and bone remodeling [12].

Cao et al. were the first to examine the osteogenic potential of the BMHP1 motif on mesenchymal stem cells (MSCs) [13]. The BMHP1 motif targeting bone marrow and binding to stem cells [14], further stabilizing its biological activity while occupying less space than its native protein [15]. Research suggests that physically entrapping motifs within 3D scaffolds enhances their biological activity [16]. Thus, binding the BMHP1 motif to (RADA)4 or KSL using two glycine spacers may increase its biological capacity. In a previous study, it was demonstrated that RADA-BMHP1 enhances bone regeneration. This current study aims to investigate which self-assembling peptide nanofiber core, RADA or KSL, more effectively induces bone regeneration. To achieve this, the BMHP1 motif was attached to (RADA)4 and (KSL)4 through two glycine spacers. Rat bone marrow-derived MSCs were separately encapsulated in the two self-assembling peptide nanofiber hydrogel-based scaffolds to assess osteogenesis in vitro. The nanofibers were then implanted into a rat bone defect model to evaluate its osteoconductivity and potential for bone repair.

2. Materials and methods

2.1. Oligopeptide characterization: reverse phase HPLC

The oligopeptides, RADARADARADARADAGGPFSSTKT and KSLSLSLRGSLSLSLKGGPFSSTKT, were synthesized using a solid-phase synthesis method. Their molecular weight was determined

using LC-Mass and purity was subsequently confirmed using a reverse-phase HPLC method. Specifically, a 20 μl solution of the oligopeptides was injected into a SHIMADZU Inertsil ODS-SP column (4.6*250 mm*5 μm). Pump A contained 0.1 % trifluoroacetic acid in 100 % water, while pump B contained 0.1 % trifluoroacetic acid in 100 % acetonitrile, with a flow rate of 1 ml/min. Detection was performed at a wavelength of 220 nm.

2.2. In-vitro study

2.2.1. Cell metabolic activity via MTT assay

In this study, rat mesenchymal stem cells (RMSCs) were obtained from bone marrow and confirmed by flow cytometry after three passages. The researchers aimed to evaluate the metabolic activity and proliferation of RMSCs that were encapsulated in nanofibers, using an MTT assay. To conduct the assay, RMSCs were encapsulated in triplicate into RADA-BMHP1 and KSL-BMHP1 nanofibers at a final concentration of 0.125 % v/w in 96-well plates that contained DMEM-F12 (without phenol red) as a cell culture medium supplemented with 10 % FBS and 1 % Penicillin/Streptomycin. The cells were then incubated for 48 h at 37 °C in 5 % CO2 and 95 % humidity. Following the incubation period, the researchers added 3-(4,5-Dimethylthiazol-2-Yl)-2,5-Diphenyltetrazolium Bromide to each well for 4 h, followed by the addition of dimethyl sulfoxide to solubilize the formazan crystals. The absorbance was measured at 570 nm using a microplate reader for up to 20 min and subtracted from the background. The assay was performed in triplicate, and the values provided are the normalized mean ± SD of three independent experiments. The researchers note that since nanofibers can absorb the stain and induce false negatives, it is crucial to subtract the background from wells containing nanofibers without cells.

2.2.2. Cell membrane damage assay

In order to assess the potential for cellular membrane disruption caused by toxic and injurious factors, extracellular lactate dehydrogenase (LDH) levels were examined. Rat mesenchymal stem cells (RMSCs) with a density of 1 x 10^4 cells/well (passage 3) were embedded in RADA-BMHP1 and KSL-BMHP1 nanofibers at a final concentration of 0.125 % w/v and placed into 96-well plates containing Dulbecco's Modified Eagle Medium/Nutrient Mixture F-12 (DMEM-F12) without phenol red, supplemented with 10 % fetal bovine serum (FBS; GIBCO) and 1 % penicillin/streptomycin (BIO-IDEA, Iran). The cells were cultured for 48 h at 37 °C, 5 % CO2, and 95 % humidity. Subsequently, LDH levels were assessed using an LDH enzyme-linked immunosorbent assay (ELISA) kit (Roche, Germany).

In summary, after the incubation period, 100 μl of cell supernatant per well was transferred to a corresponding 96-well plate and combined with 100 μl of reaction mixture for 30 min at 22 °C. The absorbance was read at 490 nm using an ELISA reader (Bioteck). LDH release analysis was conducted in triplicate, and reported values represent the normalized mean ± standard deviation (SD) from three independent experiments.

2.2.3. Assessment of nitric oxide (NO) production

The evaluation of NO production was carried out as an indicator of osteotoxicity and osteogenesis. Rat mesenchymal stem cells (RMSCs) with a density of 1 x 10^4 cells/well (passage 3) were encapsulated into nanofibers with a final concentration of 0.125 % w/v in 96-well plates, which contained DMEM-F12 (without phenol red) as a cell culture medium, supplemented with 10 % FBS (GIBCO), and 1 % Penicillin/Streptomycin (BIO-IDEA, Iran). The cells were cultured for 48 h at 37 °C in an atmosphere containing 5 % CO2 and 95 % humidity. Afterward, 100 μl of cell supernatant was added to parallel well plates, followed by an equal volume of NO dye (Cib biotech Co, Iran). Nitrite levels were measured as an indicator of total NO production, with absorbance readings taken at 570 nm using a microplate reader (Bioteck). Background absorbance was subtracted, and the assay was conducted in triplicate. The provided values represent the normalized mean ± SD from three independent experiments.

2.2.4. ALP activity

The study aimed to investigate osteogenesis in vitro and alkaline phosphatase (ALP) activity by encapsulating rat mesenchymal stem cells (RMSCs) in nanofibers and culturing them in an osteogenic differentiation medium for 14 days. The RMSCs, with a density of 2×10^4 cells/well in passage 3, were encapsulated into nanofibers at a final concentration of 0.125 % w/v and cultured in a medium containing DMEM low glucose, 10 % FBS (GIBCO), 1 % Penicillin/Streptomycin, 10 nM Dexamethasone, 50 μM Ascorbic acid, and 10 mM β-glycerophosphate in a 24-well plate. The culture media were changed every 3 days. After 14 days, the ALP activity, an enzyme involved in osteogenesis, was evaluated using an ALP assay kit (PARS AZMUN, Iran). The absorbance was read at 405 nm using a microplate reader (Bioteck). The assay was performed in triplicate, and the values provided represent the normalized mean ± SD of three independent experiments.

2.2.5. Assessment of osteogenesis at the gene level

The aim of this study was to evaluate osteogenesis at the gene level by encapsulating rat mesenchymal stem cells (RMSCs) in nanofibers and culturing them in an osteogenic differentiation medium for 14 days. In passage 3, RMSCs (5×10^4 cells/well) were encapsulated into nanofibers at a final concentration of 0.125 % w/v in an osteogenic differentiation medium. This medium consisted of DMEM low glucose, 10 % FBS (GIBCO), 1 % Penicillin/Streptomycin, 10 nM dexamethasone, 50 μM Ascorbic acid, and 10 mM β-glycerophosphate in a 6-well plate for 14 days. The medium was replaced every three days. Subsequently, to determine the differences in mRNA levels of RUNX2, ALP, Osteocalcin (OSC), and BMP2 in the differentiated cells, quantitative real-time reverse transcription PCR (qRT-PCR) was conducted. The β-Actin gene served as an internal reference gene. Total RNA was isolated using an RNX-Plus kit (Sina clon, Iran), followed by treatment with DNAse 1. A cDNA synthesis kit (Takara, Japan) was employed for synthesizing cDNA with random hexamer and oligo dt primers. The cDNA was subjected to 45 PCR cycles in a Rotor-Gene Q real-time analyzer (Corbett, Australia) using Eva Green master mix. Each reaction was carried out in duplicate, and the reported values represent the normalized mean ± SD from three independent experiments. The relative change in gene expression was calculated using the DDCt method and normalized to the β-Actin gene.

2.2.6. Calcium deposition assessment via alizarin red staining

The purpose of this experiment was to determine calcium deposition by differentiated osteoblasts using Alizarin red (ARS) staining. In brief, passage 3 RMSCs (2 x 10^4 cells/well) were encapsulated into nanofibers at a final concentration of 0.125 % w/v in an osteogenic differentiation medium. This medium contained DMEM low glucose, 10 % FBS (GIBCO), 1 % Penicillin/Streptomycin (BIO-IDEA, Iran), 10 nM dexamethasone (Sigma-Aldrich, USA), 50 μM ascorbic acid (Sigma-Aldrich, USA), and 2 mM β-glycerophosphate in a 24-well plate for 14 days. The medium was replaced every three days. To minimize the false-positive results (non-agpaitic mineralization and dystrophic mineralization) caused by β-glycerophosphate as a phosphate source in ARS staining, its concentration was reduced to 2 mM [17,18]. Once the incubation period was complete, cells were fixed with 70 % ethanol

for 10 min, and a 40 mM ARS solution was added to the wells for 5 min. The wells were thoroughly washed with PBS, and 10 % acetic acid was added and incubated at 37 °C for 30 min. The absorbance was read at 450 nm using a microplate reader (Bioteck). The assay was performed in triplicate, and the values provided represent the normalized mean ± SD of three independent experiments.

2.3. In vivo investigation

2.3.1. Rat bone defect model

Based on our previously studies, nanofibers at the concentration of 0.125 % w/v was selected for in-vivo studies. The impact of nanofibers in vivo was evaluated by implanting them into a bilateral bone defect model in rat calvaria, created using a 6-mm trephine bur, as previously described [19,20]. Briefly, oligopeptide powder was dissolved in 10 % sucrose to achieve a final concentration of 0.125 % w/v. 12 male Wistar rats weighing 260 g (8–10 weeks old) were utilized in this study. The rats, obtained from the Animal Research Center at Iran University of Medical Sciences, Tehran, Iran, were housed under standard conditions with ad libitum access to food and water, as well as a 12-h light/dark cycle. The animal experiments received approval from the ethical committee of Iran University of Medical Sciences (IR.IUMS.AEC.1402.004) and animal experiment was compiled to the EU Directive 2010/63/EU guideline. The rats were randomly divided into three groups (n = 4): Group 1 and 2 received nanofiber implants, RADA- and KSL-BMHP1, respectively while group 3 served as the control group with no implantation. Sixty days post-implantation, the rats were sacrificed via CO2 asphyxiation, and the calvaria bone and surrounding bone tissue were excised and fixed in 10 % natural buffered formalin for one week. The bone tissue was decalcified using 14 % EDTA for 30 days and then prepared for histological evaluations.

2.3.2. Gene analysis via qRT-PCR

Sixty days after the surgery, general anesthesia was induced by intraperitoneal injection of ketamine hydrochloride (Alfason) and xylazine (Alfason) at a dosage of 5 mg/kg body weight (4:1 ratio). Bone cavities were created using a 6-mm trephine bur and promptly transferred to −196 °C after being soaked in RNX-plus. Bone sections were homogenized, and total RNA was extracted using an RNX-Plus kit (Sina Clon, Iran). Subsequently, DNAse 1 treatment was administered, and random hexamer and oligo dt primed cDNA synthesis was conducted using a cDNA synthesis kit (Takara, Japan). The cDNA was employed for 45-cycle PCR in a Rotor-gene Q real-time analyzer (Corbett, Australia) with Eva Green master mix. Each duplicate reaction was performed three times, and the relative fold change in gene expression was quantified using the DDCt method. The β-Actin gene was chosen as an internal control gene, and the primer sequences for β-Actin, Runx2, ALP, OSC, and BMP2 have been previously mentioned.

2.3.3. Bone densitometry assessment via X-ray

Eight weeks after the surgery, rats from three groups, including the control and those implanted with RADA- and KSL-BMHP1 nanofibers, were sacrificed using CO2 asphyxiation and examined with X-ray radiography. Rat calvaria were fixed in a 10 % natural buffered formalin solution. An X-ray device was employed to obtain rat calvaria radiographs. Bone mineral density was assessed at eight weeks post-surgery and compared to the control group.

2.3.4. Histological examination using H&E, Masson's trichrome, and Wright-Giemsa staining

For histological analysis, specimens were fixed in 10 % natural buffered formalin and then decalcified using 14 % EDTA for two weeks. Tissue preparation involved dehydration (a series of ethanol washes), xylene incubation (3 h), and paraffin wax immersion (60 °C, 1 h). After embedding in paraffin wax, 7 μm sections were prepared for H&E (Hematoxylin and Eosin), Masson's trichrome, and Wright-Giemsa staining. Subsequently, the slides were mounted with entellan, and images were captured using an inverted microscope (Olympus AX-800) connected to a digital camera (Leica, DC200).

2.3.4.1. Statistical analysis. GraphPad Prism V9 software was employed for analyzing data related to MTT assay, LDH release, NO production, ALP assay, gene expression, and bone density percentage in the defect sites. One Way ANOVA test was employed to compare results and determine statistical significance, with $P < 0.05$ deemed statistically significant.

3. Results

3.1. Oligopeptide characterization

The molecular formulas for R-BMHP1 and KSL-BMHP1 were C102H168N38O38 and C114H198N32O36, respectively. The Wimley-White whole-residue hydrophobicity values for the peptides (representing the sum of the whole-residue free energy of transfer for the peptides from water to the POPC interface) were 10.39 and 1.09. These data were obtained from vari ous sources, including BioSynthesis (https://www.biosyn.com), www.pepcalc.com, www.novoprolabs.com, www.aps.unmc.edu/prediction/predict, and http://biotools.nubic.northwestern.edu/. Oligopeptide characteristics are presented in Table 1.

Molecular weight and purity of the oligopeptides were assessed using liquid chromatography-mass spectrometry (LC-MS) and reverse-phase high-performance liquid chromatography (RP-HPLC) techniques. LC-Mass spectrometry results demonstrated that the oligopeptide's molecular weight closely matched the estimated molecular weight calculated by peptide2.com. Furthermore, the RP-HPLC analysis yielded a single, narrow peak, signifying the high purity of the oligopeptides (Fig. 1).

3.2. In vitro findings

3.2.1. Cell metabolic activity through MTT assay

The study compared the effects of two distinct self-assembling peptide nanofibers, KSL-BMHP1 and RADA-BMHP1, along with a control group, on cell viability and metabolic activity. The findings revealed that KSL-BMHP1 significantly enhanced cell viability and metabolic activity compared to RADA-BMHP1 ($P < 0.05$) and the control groups ($P < 0.001$). Conversely, cells encapsulated in RADA-BMHP1 nanofibers exhibited significantly higher cell viability relative to the control group ($P < 0.001$).

3.2.2. Cell membrane damage assessment

To evaluate the extent of lytic cell death and cell membrane damage, lactate dehydrogenase (LDH) was utilized as an indicator of cytosolic enzyme release into the extracellular medium. As illustrated in Fig. 2b, KSL-BMHP1 induced significantly less cell membrane damage in RMSCs compared to RADA-BMHP1 ($P < 0.001$) and the control group ($P < 0.01$). In contrast, RMSCs encapsulated in RADA-BMHP1 exhibited a significantly increased LDH release compared to the control group ($P < 0.001$) after 24 h.

3.2.3. NO production

Nitric oxide (NO) functions as a marker of toxicity and is involved in osteogenesis, affecting cell proliferation, metabolism, and differentiation based on its concentration and origin [23]. NO

Table 1
Characteristics of RADA-BMHP1 and KSL-BMHP1 oligopeptides.

	Brutto formula	Molecular weight (g/mol)	Estimated Molecular weight (g/mol)	Protein-binding Potential (Boman index: kcal/mol)	Theorical isoelectric point	Net charge in pH 7	Grand average of hydropathy	Hydrophobic ratio %	Estimated water solubility	Approximate volume (nm^3)
RADA-BMHP1	C102H168N38O38	2255.35	2575.81	3.7	10.08	+1	−0.964	36	Good	3.067
KSL-BMHP1	C114H198N32O36	2593.02	2592.99	1.14	11.73	+4	−0.048	28	Good	3.088

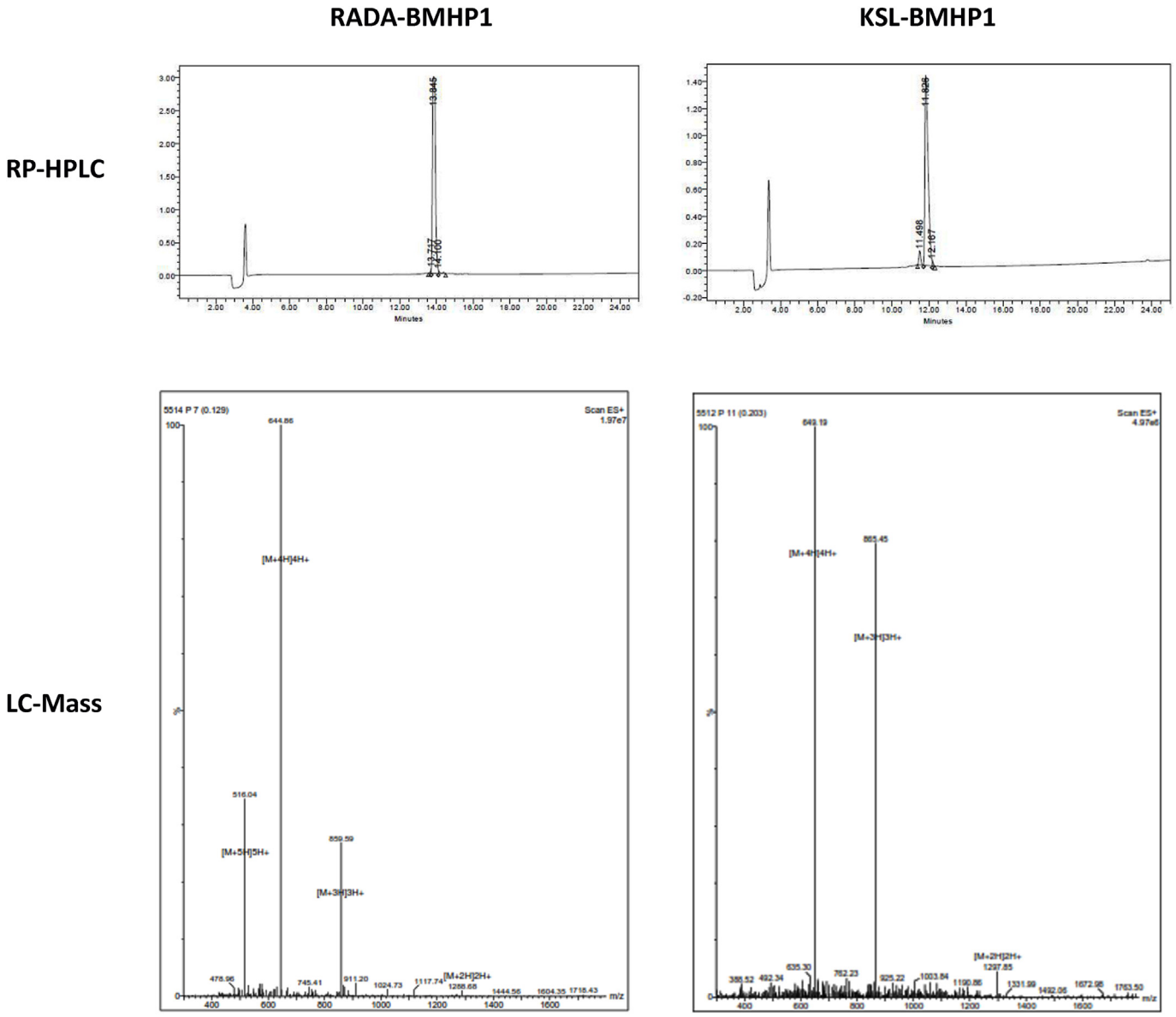

Fig. 1. RP-HPLC and Mass spectroscopy graph graphs related to RADA-BMHP1 and KSL-BMHP1.

levels were determined by measuring nitrate concentrations in the cell culture medium. The findings demonstrated that KSL-BMHP1 significantly increased NO production in RMSCs compared to RADA-BMHP1 and control groups ($P < 0.001$). However, no significant difference was observed between the nitrate levels of cells encapsulated in RADA-BMHP1 and the control group after 24 h ($P > 0.05$) (Fig. 2c).

3.2.4. Gene expression analysis by qRT-PCR in vitro

To quantify the differences in fold change gene expression in osteoblast-like cells derived from RBMSCs, cells encapsulated within self-assembling peptide nanofibers were analyzed after 14 days of differentiation. The results revealed significantly elevated RUNX2 expression in cells encapsulated in RADA-BMHP1 ($P < 0.0001$). Additionally, there were significant differences in

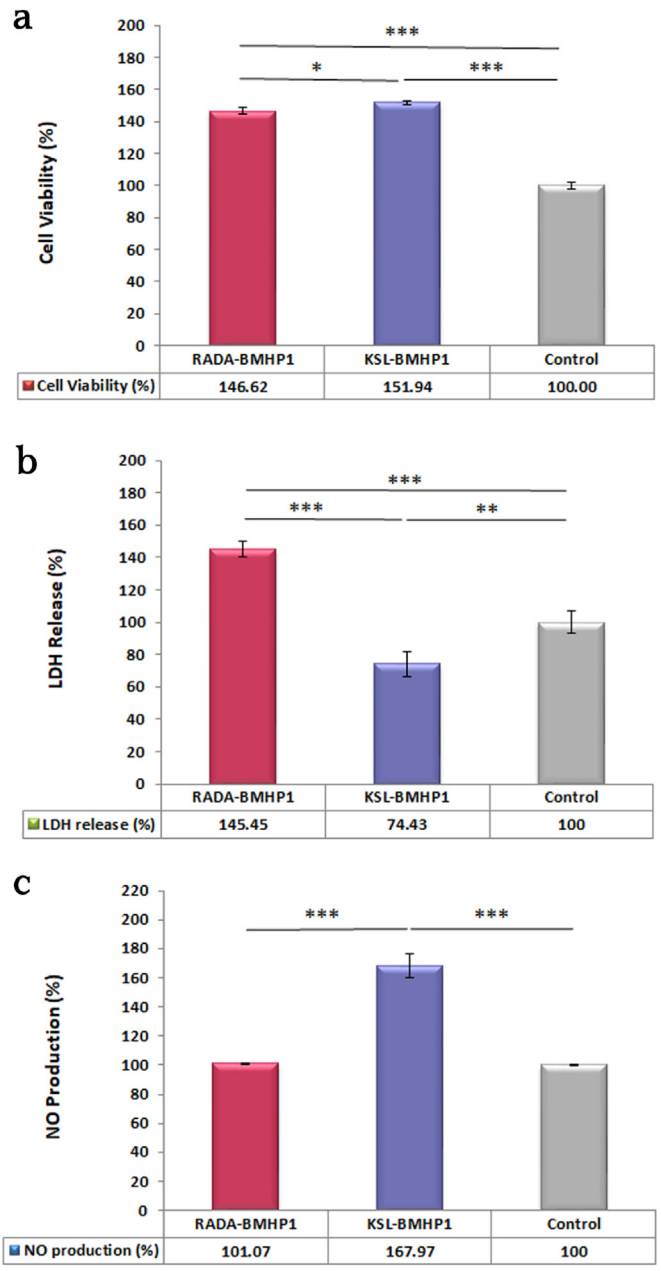

Fig. 2. Data from various experiments regarding the encapsulation of rBMSCs into self-assembling peptide nanofibers, specifically RADA-BMHP1 and KSL-BMHP1. a) shows data from an MTT assay that measures cell viability, indicating that both RADA-BMHP1 and KSL-BMHP1 results in higher cell viability compared to the control group by 48 h. b) shows data from LDH release assays, which measure the extent of cell membrane damage. The results indicate that KSL-BMHP1 induces less cell membrane damage compared to RADA-BMHP1 and the control group at 24 h. c) shows data from NO production assays, which measure the amount of nitric oxide produced. The results indicate that KSL-BMHP1 induces less cell membrane damage compared to RADA-BMHP1 and the control group at 24 h. In all panels, "***" indicates $p < 0.0001$, which means the differences between groups are statistically significant. "ns" indicates non-significant differences. The RADA-BMHP1 and KSL-BMHP1 nanofibers are colored using Pantone 2023 (BE3455) and 2022 (6868 ab) colors, respectively.

BMP2, COL1, ALP, and OSC gene expression between cells encapsulated in RADA-BMHP1 and the control group at day 14. These genes were significantly upregulated compared to the control group, with statistical analysis showing increased expression of BMP2 ($P < 0.001$), COL1 ($P < 0.0001$), ALP ($P < 0.0001$), and OSC ($P = 0.0011$) (Fig. 3a). In contrast, all gene expression levels were significantly reduced in cells encapsulated in KSL-BMHP1 compared to RADA-BMHP1 ($P < 0.001$). RUNX2, ALP, OSC, and BMP2 gene expression levels were significantly lower than the control group ($P < 0.001$) in KSL-BMHP1, while no significant difference was detected in COL1 gene expression between KSL-BMHP1 and the control group ($P > 0.05$).

3.2.5. ALP activity measurement in vitro

ALP activity, serving as an osteogenesis index, was evaluated after 14 days of differentiation. The analysis of ALP activity demonstrated that cells encapsulated in RADA-BMHP1 displayed significantly higher ALP activity than those in KSL-BMHP1 and the control group ($P = 0.0344$). In contrast, no significant difference was observed between the ALP activity levels in KSL-BMHP1 and the control group ($P > 0.05$) (Fig. 3b).

3.2.6. ARS staining

ARS staining was conducted as a matrix mineralization assay on RMSCs encapsulated in self-assembling peptide nanofibers. Images indicated that while cells supplemented with osteogenic media exhibited minimal mineral nodule formation, BMHP1 nanofibers significantly induced mineral nodule formation compared to the control group with osteogenic media at day 14 (Fig. 3c). Quantitative analysis demonstrated significantly higher matrix mineralization in RADA-BMHP1 than in KSL-BMHP1 and control groups ($P < 0.05$). Additionally, cells encapsulated in both self-assembling peptide nanofibers displayed significantly enhanced matrix mineralization compared to the control group ($P < 0.0001$) (Fig. 3d).

3.3. In vivo investigation

3.3.1. Gene expression analysis by qRT-PCR in vivo

A qRT-PCR assay was performed on cells within the defect site for self-assembling peptide nanofibers implanted for two months. The results revealed a significantly enhanced expression of RUNX2 in the KSL-BMHP1 group compared to RADA-BMHP1 and the control groups ($P < 0.05$). Additionally, BMP2, ALP, and OSC were significantly overexpressed in rats implanted with RADA-BMHP1 and KSL-BMHP1 compared to the control group two months post-implantation. The statistical analysis indicated increased expression of BMP2 ($P < 0.01$), ALP ($P < 0.0001$), and OSC ($P < 0.05$). Although there was no significant difference in ALP levels between the two self-assembling peptide nanofibers, OSC was significantly overexpressed in KSL-BMHP1 compared to RADA-BMHP1. BMP2 was significantly overexpressed in RADA-BMHP1 compared to the control group (Fig. 4a).

3.3.2. ALP activity measurement in vivo

ALP activity, an indicator of osteogenesis, was assessed in a rat bone defect model after two months. Although ALP activity significantly increased in rats implanted with KSL-BMHP1compared to the control group two months post-implantation ($P = 0.0114$), no significant difference was detected between the ALP levels in the sera of rats implanted with RADA-BMHP1 and KSL-BMHP1 ($P = 0.0405$) (Fig. 4b).

3.3.3. Bone densitometry measurements by X-ray

X-ray imaging was conducted to assess the extent of new bone formation at the defect site eight weeks post-operation. Bone mineral density data derived from X-ray demonstrated increased consolidation of new bone formation in the defect site implanted with nanofibers compared to the control group ($P < 0.05$). RADA-BMHP1 significantly promoted higher bone formation than KSL-BMHP1 ($P < 0.05$). In other words, data revealed a significant increase in bone mineral density using nanofibers (Fig. 4c and d).

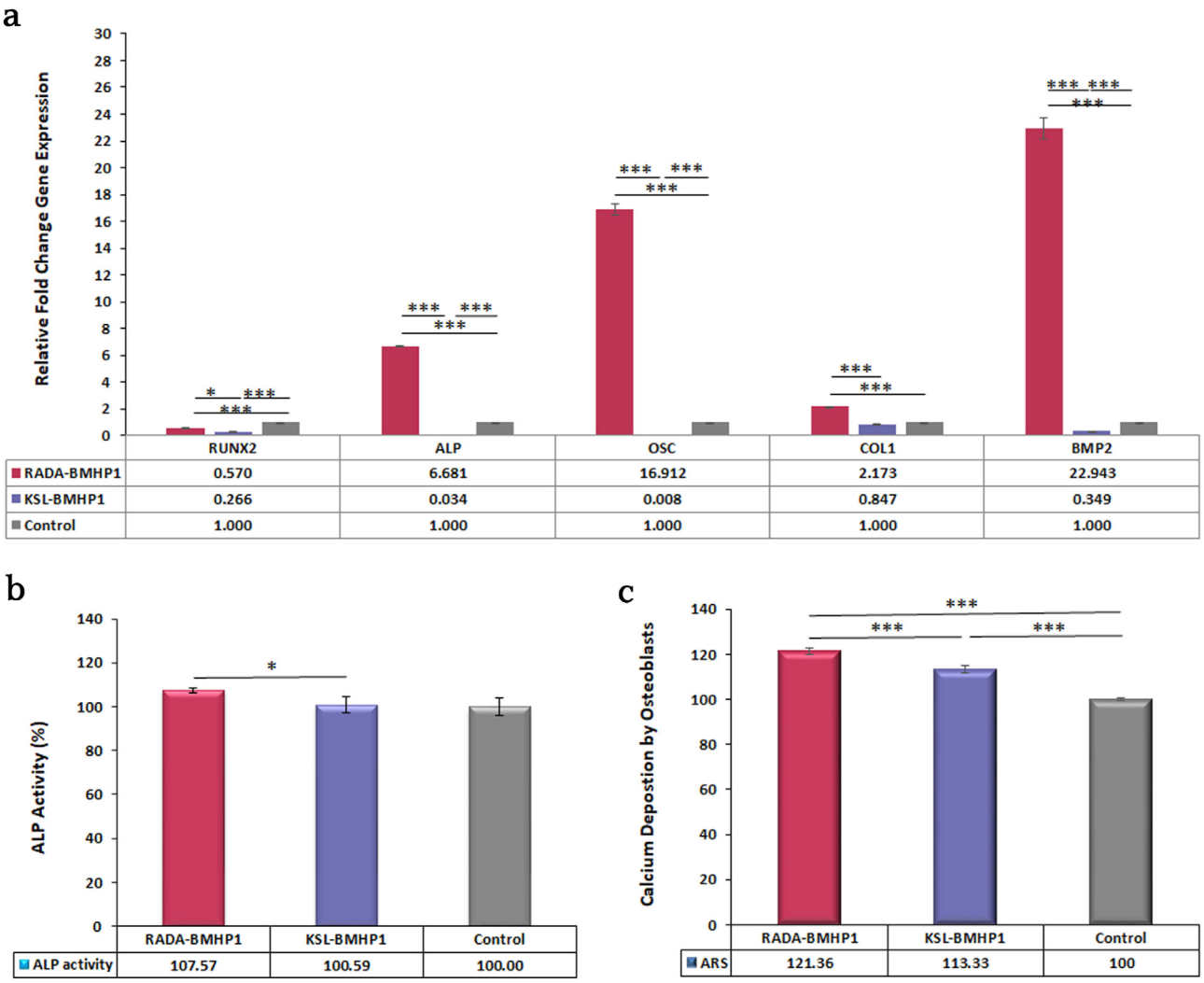

Fig. 3. a) Relative fold change gene expression of osteogenic markers including RUNX2, BMP2, COL1, ALP, and OSC. Data showed that RADA-BMHP1 nanofiber induced significantly higher genes over-expression than the KSL-BMHP1 nanofiber and control group. b) ALP activity of rBMSCs encapsulated into RADA-BMHP1, KSL-BMHP1 nanofibers supplemented with osteogenic media by 14 days. Results showed higher ALP activity in osteoblast-like cells derived from rBMSCs encapsulated into RADA-BMHP1 nanofiber than the KSL-BMHP1 and the control group. c) The quantitative analysis of calcium deposition by the osteoblasts staining by Alizarin Red staining. Results indicated that RADA-BMHP1, KSL-BMHP1 nanofibers induced significantly higher calcium deposition than the control group. "***" means $p < 0.0001$, "**" means $p < 0.01$, "*" means $p < 0.05$.

3.3.4. Histological evaluation by H&E, Masson's trichrome and Wright-Giemsa staining

H&E staining in the control group showed a loose fibrous connective tissue in defect site with the scanty bone marrow cavity and a few small islands of new bone on the periphery. While implantation of RADA-BMHP1 nanofibers had been led to an increased new bone integration with original bone tissue. Although it was observed some bone marrow cavities in the defect, loose connective tissue was going to disappear and was placed with the mature bone tissue containing osteocytes within lacunae. There was no sign of BMHP1 nanofibers in defect and osteoblasts were arranged in a regular row at the margin of new bone (Fig. 5). Although, KSL-BMHP1 had induced significantly bone regeneration compared to the control group, its bone regeneration potential was less than the RADA-BMHP1 nanofibers. In other words, KSL-BMHP1 showed higher connective tissue and less hard tissue than the RADA-BMHP1.

Masson's trichrome staining in bone defect implanted with BMHP1 nanofibers showed new bone formation with mature bone tissue (red staining) than the control group. Moreover, Staining of KSL-BMHP1 specimens showed higher amount of collagen fibers, blue staining, and less mature bone tissue (red staining) than the RADA-BMHP1 (Fig. 5).

Interestingly, Wright-Giemsa staining did not show any polymorphonuclear cells as a cell involves in inflammation at the margin and periphery of a bone defect in an implanted defect that confirmed bio-compatibility of RADA-BMHP1 and KSL-BMHP1 nanofibers as the scaffolds and bone substitute for bone repair (Fig. 5).

4. Discussion

Bone tissue engineering aims to develop functional biomaterials that can promote bone regeneration, particularly in cases of critical-sized bone defects or diseases that impair bone formation. Self-assembling peptide nanofibers represent a promising platform for bone tissue engineering due to their biocompatibility, biodegradability, and ability to mimic the natural extracellular matrix (ECM) environment, which is crucial for cell adhesion, proliferation, and differentiation. Moreover, the tunable physicochemical properties of these peptide nanofibers, such as hydrophobicity, net charge, and protein-binding potential, can be tailored to optimize their

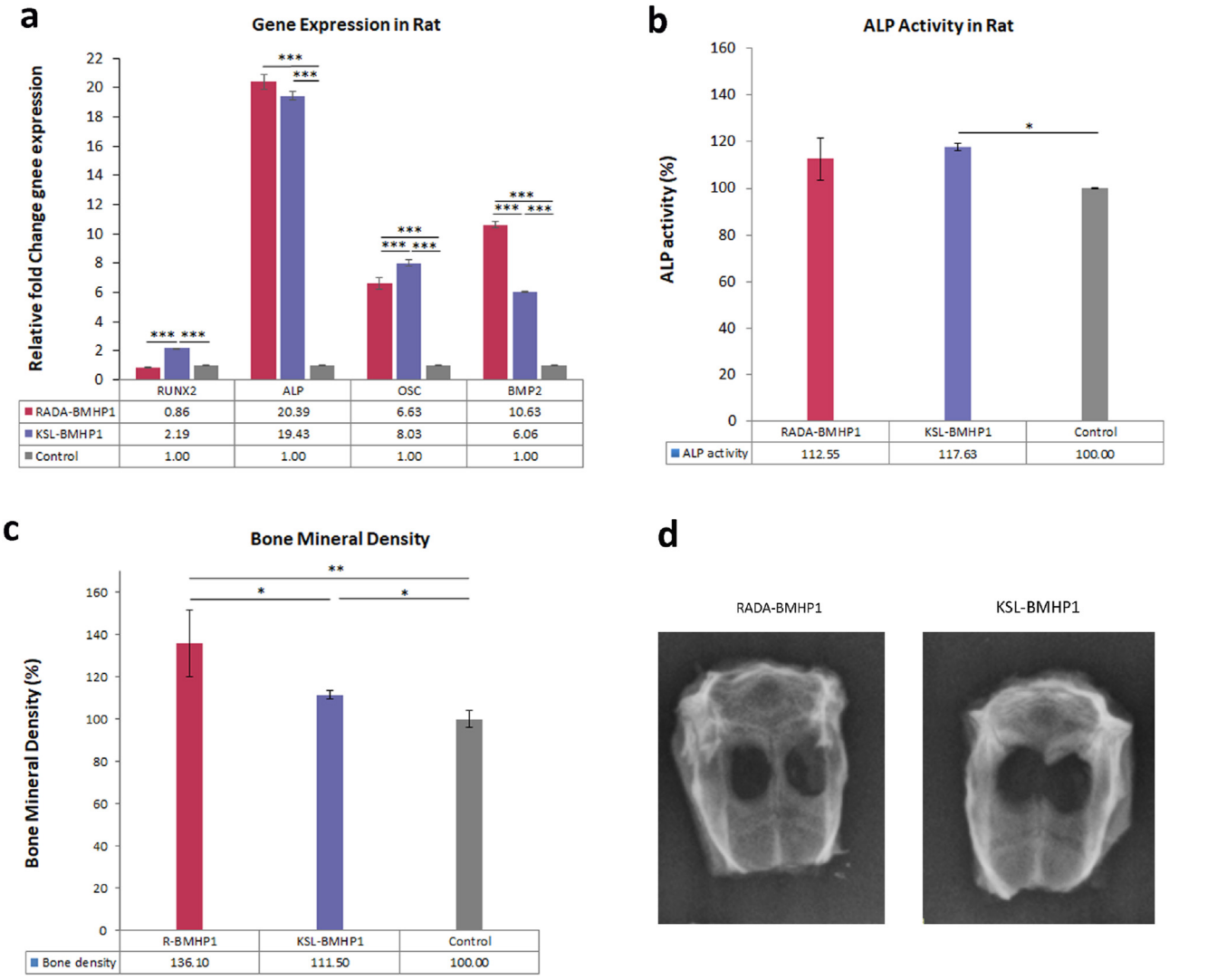

Fig. 4. a) Relative fold change gene expression of bone markers including RUNX2, BMP2, ALP and OSC in the implanted bone defect and the empty control group. Data showed that implantation of RADA-BMHP1 and KSL-BMHP1 nanofibers induced significantly higher genes over-expression than the control group by 60 days post-implantation. b) ALP activity in serum of rats implanted with of RADA-BMHP1 and KSL-BMHP1 nanofibers by 60 days post-implantation. Results showed higher ALP activity in serum of rats implanted with KSL-BMHP1 than the control group. c) Analysis of bone mineral density derived from X-ray graphs relating to the control group and RADA-BMHP1 and KSL-BMHP1 nanofibers implanted into the rat calvarial cavities by 60 days. d) X-Ray graphs of RADA-BMHP1 and KSL-BMHP1 nanofibers implanted into the rat calvaria cavities by 60 days "***" means $p < 0.0001$, "**" means $p < 0.01$, "*" means $p < 0.05$.

interaction with cells and ECM components, thereby modulating cellular behavior and tissue regeneration outcomes.

In this study, the osteogenic potential of two self-assembling peptide nanofibers, RADA-BMHP1 and KSL-BMHP1, both in vitro and in vivo was investigated. The results demonstrated that RADA-BMHP1 significantly enhanced osteogenic differentiation and matrix mineralization in rMSCs, whereas KSL-BMHP1 showed superior cell viability and reduced cell membrane damage. In vivo experiments revealed that both self-assembling peptide nanofibers improved bone regeneration in a rat bone defect model, with RADA-BMHP1 showing a greater increase in bone formation compared to KSL-BMHP1.

The molecular characteristics of the peptides, such as their molecular weight, estimated molecular weight, protein-binding potential, grand average of hydropathy, theoretical isoelectric point, and net charge at pH 7, were assessed using various sources. Both oligopeptides displayed high purity and molecular weights that closely matched their estimated values, suggesting that these peptides were suitable for further investigation.

The in vitro results demonstrated that cells encapsulated in KSL-BMHP1 nanofibers exhibited significantly higher cell viability as evidenced by the MTT assay data compared to the RADA-BMHP1 and the control group. Additionally, KSL-BMHP1 induced less cell membrane damage in rMSCs compared to RADA-BMHP1 and the control group. These findings indicate that KSL-BMHP1 provides a more favorable microenvironment for cell survival and growth, which may be attributed to its lower hydrophobicity value and higher net charge at pH 7 compared to RADA-BMHP1. In contrast, RADA-BMHP1 exhibited superior osteogenic differentiation properties, as evidenced by the upregulation of osteogenic genes (RUNX2, BMP2, COL1, ALP, and OSC) and increased ALP activity and matrix mineralization in rMSCs. The enhanced osteogenic potential of RADA-BMHP1 may be due to its higher protein-binding potential and grand average of hydropathy compared to KSL-BMHP1, which

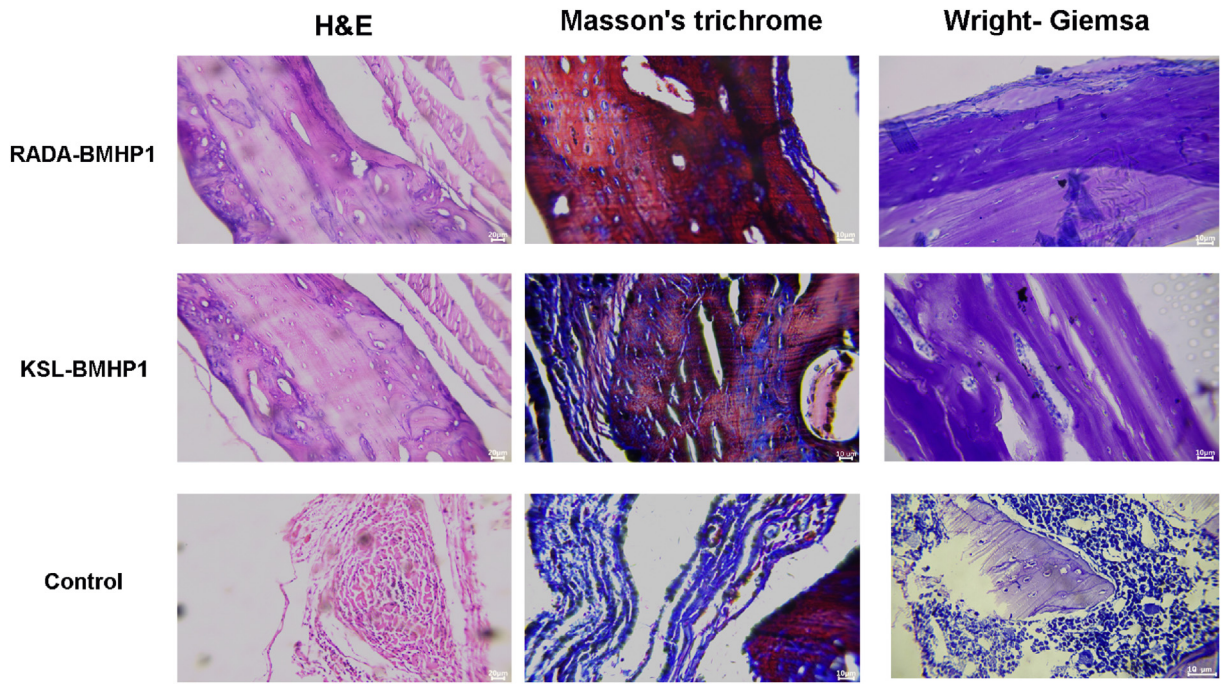

Fig. 5. H&E, Masson's trichrome and Wright-Giemsa staining in bone defect implanted with RADA-BMHP1, KSL-BMHP1 nanofibers and the control group. Data showed higher bone regeneration potential of RADA-BMHP1 than the KSL-BMHP1 nanofibers.

could facilitate the interaction between the peptide nanofibers and proteins involved in osteogenesis. Furthermore, the upregulation of BMP2, a critical growth factor for osteogenesis, may contribute to the enhanced osteogenic differentiation observed in cells encapsulated in RADA-BMHP1.

The MTT assay data indicated that KSL and RADA-BMHP1 nanofibers enhanced MSCs viability, while RADA-BMHP1 eventually elevating LDH release probably through its acidic nature. Notwithstanding, acidic pH microenvironment of osteoblasts can promote autophagy to enhance osteoblast survival and preventing osteoblast apoptosis [21]; therefore the acidic pH of RADA-BMHP1 did not decreased cell viability and had no adverse effect on NO production. NO data demonstrated that KSL-BMHP1 significantly increased NO production in MSCs compared to RADA-BMHP1 and the control groups. NO plays a dual role in osteogenesis, acting as both a pro-osteogenic and anti-osteogenic agent, depending on its concentration and origin. At low levels, NO has been shown to promote cell proliferation, and differentiation, while high levels of NO can induce cytotoxic effects and inhibit osteogenic differentiation [22–24]. Therefore, the modulation of NO production by KSL-BMHP1 could have contributed to its enhanced cell viability and metabolic activity compared to RADA-BMHP1. However, further studies are needed to elucidate the underlying mechanisms by which KSL-BMHP1 modulates NO production and its impact on cellular behavior and bone tissue engineering applications.

Runx2, COL1, BMP2, ALP, and OSC are five major and critical genes involved in osteogenesis. When, ALP, produced free phosphate, OSC sequestering calcium for mineralization and this cooperation leading to osteogenesisn [6]. RADA-BMHP1 nanofiber significantly increased the BMP2, Runx2, COL1, ALP, and OSC at the mRNA level in rBMSC. Moreover, ALP activity showed an increment in cells in in-vitro and in the serum of rats. Besides of ALP activity and over-expression of OSC, quantitative alizarin red assay confirmed significantly enhanced mineralization in RADA-BMHP1 nanofibers compared to the KSL-BMHP1 and the control group.

To validate the in vitro findings, he in vivo experiments conducted in a rat bone defect model, in which the self-assembling peptide nanofibers, RADA-BMHP1 and KSL-BMHP1, were implanted into the defect site for two months. The results revealed that both RADA-BMHP1 and KSL-BMHP1 improved bone regeneration, with RADA-BMHP1 showing a greater increase in bone formation compared to KSL-BMHP1, as evidenced by gene expression analysis, ALP activity measurement, bone densitometry measurements by X-ray, and histological evaluation. The histological evaluation revealed better integration of new bone tissue with the original bone and the absence of any inflammation, indicating the biocompatibility of both self-assembling peptide nanofibers as scaffolds for bone repair. However, the bone regeneration potential of RADA-BMHP1 was significantly higher than the KSL-BMHP1.

These findings suggest that RADA-BMHP1 may be a more suitable candidate for bone tissue engineering applications due to its superior osteogenic potential.

The superior osteogenesis potential of RADA-BMHP1 was consistent with our earlier docking and MD studies, where they showed a high minus binding energy derived from binding of RADA-BMHP1 to BMPR1A. Noteworthy, the total binding energy of BMP2 to BMPR1A was higher than RADA-BMHP1 while the electrostatic energy of RADA-BMHP1 to the BMPR1A was more negative than BMP2. It appears that the positive polar solvation energy was responsible for the less negative binding energy of RADA-BMHP1 and if one designed an RADA-BMHP1 nanofiber in which its residues have less polar solvation energy in interaction with BMPR1A, it will more efficient than BMP2 [25]. Cell-cell communication has critical role in promoting osteogenesis and bone remodeling, therefore, an strong cell adhesion is a key factors in triggering mature bone regeneration. RADA-BMHP1and KSL-BMHP1 are rich in a positively charged amino acid of arginine (R) and lysine (K) promoting cell adhesion at the onset of cell recognition [26]. We previously showed that arginine and lysine residues have strong interaction to BMPR1A resulting in triggering of BMP2 cell signaling cascade [25].

The activation of the BMP2 receptor is crucial for the proper development of bone tissue. This activation leads to the phosphorylation of a specific protein called Smad 1/5. As a result, the gene called Runx2 is overexpressed, playing a central role in the formation of bone tissue [27]. Additionally, both BMP2 and integrin can stimulate the p38MAPK and JNK signaling pathways, which ultimately contribute to the process of osteogenesis, or the formation of new bone [28]. These findings confirm the strong bone regeneration potential of both KSL and RADA-BMHP1. In other side, the positively charged amino acids in both KSL and RADA-BMHP1 nanofibers interact with the cell membrane, negatively charged, to enhance cell adhesion and mobilization [3].

Beside of the chemical structures of these nanofibers in triggering osteogenesis, mechanotransduction signals derived from their nanotopography has pivotal role in enhanced bone regeneration [19,29]. Nanomaterials and nanofibers, due to their smaller size, have a higher ratio of surface area to volume compared to micrometer-sized materials. This increased surface area provides more space for proteins to be adsorbed, leading to enhanced cell recognition and adhesion [30]. This characteristic is particularly advantageous when considering the binding of the RADA-BMHP1 motif to the self-assembling core, as it allows for a greater binding capacity compared to the BMHP1 motif alone. Additionally, the nanotopography of the extracellular matrix can affect protein conformation and epitope availability, ultimately influencing the response of cells. This can result in the activation of the MAPK cascade, leading to over-expression of the RUNX2 gene and osteogenesis [31]. Yang et al. [6] found that the nanotopography promotes the colocalization of BMP2 receptor and integrin on the surface of MSCs. This colocalization leads to increased expression of the Runx2 gene and protein compared to a planar surface, as it triggers the BMP2 signaling cascade [4]. Brammer et al. demonstrated that MSCs adhere well to the 30 nm TiO2 nanotubes. However, other studies have shown that MSCs [32] and human fetal osteoblastic cells [33] preferentially adhere to 11–13 nm randomly shallow nano-islands. This enhanced adhesion is attributed to increased focal adhesions and actin fibers. However, adhesion decreases when the nano-island diameter increases to 90 nm [34]. The self-assembling peptide nanofibers are in the range of approximately 10–20 nm, which aligns well with the particle size of random shallow nano-islands (11–13 nm). This suggests that self-assembling peptide nanofibers can engage in focal adhesion and actin fiber interactions, promoting enhanced cell adhesion and proliferation. Additionally, Kilian et al. proposed that the involvement of the actomyosin machinery plays a role in MSC differentiation towards osteogenesis [35]. Given the large surface area of KSL-BMHP1 and RADA-BMHP1 nanofibers and their nanotopography they can adsorb a higher protein content, which, in turn, promotes MSC proliferation and differentiation resulting in bone regeneration.

The present study comprehensively investigated the effects of two self-assembling peptide nanofibers, RADA-BMHP1 and KSL-BMHP1, on the viability, osteogenic differentiation, and bone regeneration properties of rat mesenchymal stem cells (rMSCs). The results of our study offer valuable insights into the differential effects of these peptide nanofibers on cellular behavior and bone tissue engineering applications. Furthermore, our findings demonstrated that the bone regeneration capacity of RADA-BMHP1 (136.1 ± 13.81 %) exhibited comparability to that of demineralized bone matrix (DBM) (144.82 ± 4.09), which is widely recognized as a source of osteogenic growth factors and bone morphogenetic protein 2 (BMP2) [20]. While the study provides valuable insights into the differential effects of RADA-BMHP1 and KSL-BMHP1 on cell viability, osteogenic differentiation, and bone regeneration, some points should be considered when interpreting the findings. In addition to optimizing the physicochemical properties and functionalization of RADA-BMHP1 and KSL-BMHP1, several other research directions could be explored to further advance our understanding of self-assembling peptide nanofibers and their potential applications in bone tissue engineering and regenerative medicine. First, the incorporation of bioactive molecules or growth factors, such as bone morphogenetic proteins (BMPs) or vascular endothelial growth factor (VEGF), into the self-assembling peptide nanofibers could enhance their osteogenic and angiogenic potential, respectively, thus promoting bone regeneration and vascularization in the defect site. Moreover, the conjugation of other cell-adhesive motifs, to the peptide nanofibers could improve cell adhesion, spreading, and proliferation, further enhancing their performance in bone tissue engineering applications.

Second, the development of composite biomaterials that combine self-assembling peptide nanofibers with other materials, such as biodegradable polymers, ceramics, or metals, could provide synergistic effects in terms of mechanical properties, bioactivity, and biodegradability, resulting in improved bone regeneration outcomes. For example, composite materials consisting of peptide nanofibers and nano-hydroxyapatite, a naturally occurring mineral component of bone, could mimic the native bone ECM more closely, thereby supporting cell adhesion, proliferation, and differentiation, as well as promoting the formation of new bone tissue.

Third, the application of advanced fabrication techniques, such as 3D bioprinting, could enable the development of self-assembling peptide nanofiber-based constructs with precisely controlled architecture and mechanical properties, tailored to the specific requirements of the bone defect or tissue engineering application. Such constructs could provide a more accurate replication of the native bone ECM and mechanical environment, thus promoting cellular behavior and tissue regeneration.

Lastly, the exploration of additional self-assembling peptide nanofiber sequences with diverse physicochemical properties, bioactivity, and functionalization potential could expand the toolbox of biomaterials available for bone tissue engineering and regenerative medicine applications.

5. Conclusion

The discovery and development of novel peptide nanofiber sequences with enhanced biocompatibility, osteogenic potential, and functional versatility could lead to the design of next-generation biomaterials with improved performance and clinical applicability. The present study demonstrates that RADA-BMHP1 and KSL-BMHP1 possess distinct properties that differentially impact cell viability, osteogenic differentiation, and bone regeneration. While KSL-BMHP1 provides a more favorable environment for cell survival and growth, RADA-BMHP1 exhibits superior osteogenic potential, making it a more suitable candidate for bone tissue engineering applications. Further research is warranted to elucidate the underlying molecular mechanisms responsible for the observed differences in the osteogenic properties of these self-assembling peptide nanofibers and to explore their potential use in combination therapies for more effective bone regeneration.

Author's contribution

B. R was contributed in animal studies and formal analysis, Z. S and M.H.H.T were contributed in oligopeptide synthesis, S.C was contributed in tissue preparation, pathological investigations and, data curation E.H was contributed in in-vitro studies, data curation, validation and original draft writing, S.M.R. was contributed in investigation and validation and writing, S.T was contributed in

conceptualization, supervision, funding acquisition, resources, validation and original draft writing - review & editing.

Funding and acknowledgment

This work was supported by the grants from “Iran University of Medical Sciences, Tehran, Iran (grant numbers 1401-4-99-25267 and 1403-3-99-31280).

Data availability

The raw data supporting the conclusions of this article will be made available by the authors on request.

Declaration of competing interest

The authors declare that they have no known competing financial interests or personal relationships that could have appeared to influence the work reported in this paper.

References

[1] Fukuba S, Okada M, Nohara K, Iwata TJM. Alloplastic bone substitutes for periodontal and bone regeneration in dentistry: current status and prospects, vol. 14; 2021. p. 1096.
[2] futuremarketinsights. Bone grafts and substitutes market in futuremarketinsights. 2022.
[3] Ando K, Imagama S, Kobayashi K, Ito K, Tsushima M, Morozumi M, et al. Effects of a self-assembling peptide as a scaffold on bone formation in a defect. PLoS One 2018;13:e0190833.
[4] Marí-Buyé N, Luque T, Navajas D, Semino CE. Development of a three-dimensional bone-like construct in a soft self-assembling peptide matrix. Tissue Eng 2013;19:870–81.
[5] Spirio L, Hasturk H, Dyke TV. Implanting tools or instruments for sinus lifting. 2017 (US).
[6] Yang J, McNamara LE, Gadegaard N, Alakpa EV, Burgess KV, Meek RD, et al. Nanotopographical induction of osteogenesis through adhesion, bone morphogenic protein cosignaling, and regulation of microRNAs. ACS Nano 2014;8:9941–53.
[7] Salmasi S, Kalaskar DM, Yoon W-W, Blunn GW, Seifalian AM. Role of nanotopography in the development of tissue engineered 3D organs and tissues using mesenchymal stem cells. World J Stem Cell 2015;7:266.
[8] Janson IA. Investigating the roles of matrix nanotopography and elasticity in the osteogenic differentiation of mesenchymal. Stem Cell 2014.
[9] Tavakol S, Saber R, Hoveizi E, Tavakol B, Aligholi H, Ai J, et al. Self-assembling peptide nanofiber containing long motif of laminin induces neural differentiation, tubulin polymerization, and neurogenesis: in vitro, ex vivo, and in vivo studies. Mol Neurobiol 2016;53:5288–99.
[10] Tavakol S, Musavi SMM, Tavakol B, Hoveizi E, Ai J, Rezayat SM. Noggin along with a self-assembling peptide nanofiber containing long motif of laminin induces tyrosine hydroxylase gene expression. Mol Neurobiol 2017;54:4609–16.
[11] Tavakol S, Saber R, Hoveizi E, Aligholi H, Ai J, Rezayat SM. Chimeric self-assembling nanofiber containing bone marrow homing peptide's motif induces motor neuron recovery in animal model of chronic spinal cord injury; an in vitro and in vivo investigation. Mol Neurobiol 2016;53:3298–308.
[12] Civitelli R. Cell–cell communication in the osteoblast/osteocyte lineage. Arch Biochem Biophys 2008;473:188–92.
[13] Cao F-Y, Yin W-N, Fan J-X, Zhuo R-X, Zhang X-Z. A novel function of BMHP1 and cBMHP1 peptides to induce the osteogenic differentiation of mesenchymal stem cells. Biomater Sci 2015;3:345–51.
[14] Nowakowski GS, Dooner MS, Valinski HM, Mihaliak AM, Quesenberry PJ, Becker PS. A specific heptapeptide from a phage display peptide library homes to bone marrow and binds to primitive hematopoietic stem cells. Stem Cell 2004;22:1030–8.
[15] Hersel U, Dahmen C, Kessler H. RGD modified polymers: biomaterials for stimulated cell adhesion and beyond. Biomaterials 2003;24:4385–415.
[16] Silva GA, Czeisler C, Niece KL, Beniash E, Harrington DA, Kessler JA, et al. Selective differentiation of neural progenitor cells by high-epitope density nanofibers. Science 2004;303:1352–5.
[17] Langenbach F, Handschel J. Effects of dexamethasone, ascorbic acid and β-glycerophosphate on the osteogenic differentiation of stem cells in vitro. Stem Cell Res Ther 2013;4:117.
[18] Chung C-H, Golub EE, Forbes E, Tokuoka T, Shapiro IM. Mechanism of action of β-glycerophosphate on bone cell mineralization. Calcif Tissue Int 1992;51:305–11.
[19] Tavakol S, Kashani IR, Azami M, Khoshzaban A, Tavakol B, Kharrazi S, et al. In vitro and in vivo investigations on bone regeneration potential of laminated hydroxyapatite/gelatin nanocomposite scaffold along with DBM. J Nanoparticle Res 2012;14:1265.
[20] Tavakol S, Khoshzaban A, Azami M, Kashani IR, Tavakol H, Yazdanifar M, et al. The effect of carrier type on bone regeneration of demineralized bone matrix in vivo. J Craniofac Surg 2013;24:2135–40.
[21] Zhang Z, Lai Q, Li Y, Xu C, Tang X, Ci J, et al. Acidic pH environment induces autophagy in osteoblasts, vol. 7; 2017. p. 46161.
[22] Wimalawansa SJ. Nitric oxide and bone, vol. 1192; 2010. p. 391–403.
[23] An SY, Lee HJ, Lee SC, Heo JSJT, Cell. Supplement of nitric oxide through calcium carbonate-based nanoparticles contributes osteogenic differentiation of mouse embryonic. Stem Cell 2020;66:101390.
[24] Nascimento MH, Pelegrino MT, Pieretti JC, Seabra ABJAMS. How can nitric oxide help osteogenesis?, vol. 7; 2020. p. 29–48.
[25] Tavakol S, Rasoulian B, Ramezani F, Hoveizi E, Tavakol B, Rezayat SMJMS, C E. Core and biological motif of self-assembling peptide nanofiber induce a stronger electrostatic interaction than BMP2 with BMP2 receptor 1A, vol. 101; 2019. p. 148–58.
[26] Schneider GB, English A, Abraham M, Zaharias R, Stanford C, Keller J. The effect of hydrogel charge density on cell attachment. Biomaterials 2004;25:3023–8.
[27] Shi Y, Massagué J. Mechanisms of TGF-β signaling from cell membrane to the nucleus. Cell 2003;113:685–700.
[28] Guicheux J, Lemonnier J, Ghayor C, Suzuki A, Palmer G, Caverzasio J. Activation of p38 mitogen-activated protein kinase and c-Jun-NH2-terminal kinase by BMP-2 and their implication in the stimulation of osteoblastic cell differentiation. J Bone Miner Res 2003;18:2060–8.
[29] Tavakol S, Nikpour MR, Hoveizi E, Tavakol B, Rezayat SM, Adabi M, et al. Investigating the effects of particle size and chemical structure on cytotoxicity and bacteriostatic potential of nano hydroxyapatite/chitosan/silica and nano hydroxyapatite/chitosan/silver; as antibacterial bone substitutes. J Nanoparticle Res 2014;16:2622.
[30] Hess C, Schwenke A, Wagener P, Franzka S, Laszlo Sajti C, Pflaum M, et al. Dose-dependent surface endothelialization and biocompatibility of polyurethane noble metal nanocomposites. J Biomed Mater Res 2014;102:1909–20.
[31] Xia Y, Chen H, Zhang F, Wang L, Chen B, Reynolds MA, et al. Injectable calcium phosphate scaffold with iron oxide nanoparticles to enhance osteogenesis via dental pulp stem cells. Artif Cell Nanomed Biotechnol 2018:1–11.
[32] Frey MT, Tsai IY, Russell TP, Hanks SK, Wang Y-l. Cellular responses to substrate topography: role of myosin II and focal adhesion kinase. Biophys J 2006;90:3774–82.
[33] Lim JY, Hansen JC, Siedlecki CA, Runt J, Donahue HJ. Human foetal osteoblastic cell response to polymer-demixed nanotopographic interfaces. J R Soc Interface 2005;2:97–108.
[34] Yang Y, Wang K, Gu X, Leong KW. Biophysical regulation of cell behavior—cross talk between substrate stiffness and nanotopography. Engineering 2017;3:36–54.
[35] Kilian KA, Bugarija B, Lahn BT, Mrksich M. Geometric cues for directing the differentiation of mesenchymal stem cells, vol. 107. Proceedings of the National Academy of Sciences; 2010. p. 4872–7.